INTEGRATING COMPACT ELECTROCHEMICAL MEASUREMENT READOUTS ON A MODULAR ORGAN-ON-CHIP PLATFORM

MASTER GRADUATION PROJECT ELECTRICAL ENGINEERING

Wouter Nijenhuis

EEMCS
BIOS - Lab on a Chip group

Committee Chair:	prof.dr.ir. Mathieu Odijk
Daily Supervisor:	Aniruddha Paul
External Examiner:	dr.ir. Dennis Alveringh

2ND DECEMBER 2024

Contents

Abstract

The demand for Organ-on-Chip systems has risen due to a shift away from animal testing and the need to make more complex cell culture systems. A modular platform is being designed using the ISO 22916:2022 standard to advocate standardization within the field. It strives to be a true lab-on-chip and not chip-in-a-lab system by integrating microfluidics and electronics within the size of a multiwells plate, which reduces the number of external connections needed. The goal of this master's project is to reduce further the external connections needed by designing a way of integrating electrochemical sensor read-out onto the modular platform. The device's design is chosen as a modular one-cable solution using the EmStat Pico module from PalmSens integrated on a PCB. The device's footprint is 35 x 38 mm and can fit on top of a 30 x 30 mm microfluidic building block. Proof-of-concept measurements are carried out using a three-electrode setup with platinum working and counter electrodes and a quasi-reference Ag/AgCl electrode. Electrical impedance spectroscopy is used to show a difference in KCl concentration. Differences in oxygen concentration are shown in cyclic voltammetry and chronoamperometry. With the device integrated on the platform, the experiments show successful electrochemical measurements for monitoring Organ-on-Chip system parameters.

1 Introduction

The development of society has paved the way for people wanting to live longer and healthier lives. This has created the need for more treatments to achieve this lifestyle. Developing these treatments is a lengthy and costly process, mainly due to the clinical trials that need to be performed[1]. For example, drugs need to be tested in an environment that closely matches its target to determine the effectiveness and side effects. This can be done in animals that have the same kind of mechanisms as the human body. These *in vivo* studies bring a lot of complexity and, therefore, uncertainty since the test environment is not precisely controlled. Furthermore, animal testing is becoming less and less desired by governing bodies due to ethics concerns[2]. To aim for quicker testing and a more controlled environment, *in vitro* methods have been designed. Here, a small sample of target tissue is tested in a controlled lab environment. In the simplicity of *in vitro* testing also lies a drawback[3]. The testing in these environments does not take into account the complex interconnected systems and environments of the human body. A solution would be to include more tissue types, simulate more accurate environments, and use those together to make the model more complex. One of the methods to make *in vitro* systems more complex is to use Organ-on-Chip (OoC) platforms[4]. With this technology, the cell cultures are made inside microfluidic devices where the physiology can be mimicked by replicating its 3D cell structure and where the environment can be precisely controlled by adding, for example, mechanical stress to the cells. Different cultures can be connected as well, making a network of multiple cell cultures to mimic the systems in the human body better.

The development of microfluidic platforms has grown in the last few years[5] but has not seen widespread adoption in clinical trials. Due to their complex and multidisciplinary nature, full OoC platforms are hard to develop by the researchers who also want to use them. Next to that, the platforms are highly specific for the tissue that is used inside of the OoC and what needs to be tested on that tissue[6]. This means that every OoC platform has different specifications and dimensions to fit the lab and the equipment that is supposed to be used. Therefore platforms and setups are hard to connect together or implement in a different location. To give more guidance in the development of microfluidic platforms (including OoC) and make it possible for manufacturers to develop modules for microfluidic systems that more researchers can use, a consortium consisting of companies and research institutes developed a standard on which these platforms can be designed[7].

While this standard is supposed to solve the issue of inter-compatibility, it is not yet widespread in use, and the complexity of fabricating the systems is not yet tackled. To advocate that the standard can be applied to OoC applications and to get a usable platform in the hands of researchers, a Starterkit is being developed at the BIOS Lab-on-a-Chip group shown in Figure 1. The Starterkit is a modular microfluidic platform for OoC applications and interconnects microfluidic building blocks with pumps and reservoirs via a customizable routing block. The goal of the Starterkit is to develop a true standalone setup by reducing the number of external microfluidic and electrical connections needed to work with and test on a microfluidic chip.

Monitoring cell cultures is important to see the effect during experiments in OoC research and the goal of the Starterkit is to have an all-in-one platform for OoC research. Therefore, the goal of this master project is to design a way of integrating electrochemical sensor read-out onto the Starterkit in a standardized and open manner, ensuring optimal signal quality and ease of use while requiring minimal external connections. This report will show the process of this project and the reasoning behind it. The background elaborates on which open standards need to be adhered to. That section will also give information about which signals will need to be processed so optimal signal quality can be ensured while moving to the design of the device. Theory about electrochemical measurements will be given so the methods and results can be understood more clearly. In the design chapter, the information from the background will be formulated as requirements, and the choices for the design will be explained. The methods for the production of the design and the proof of concept experiments are shown after. The results are shown and discussed in the next chapter to conclude the functioning of the device. The last chapter of this report introduces future design choices and experiments.

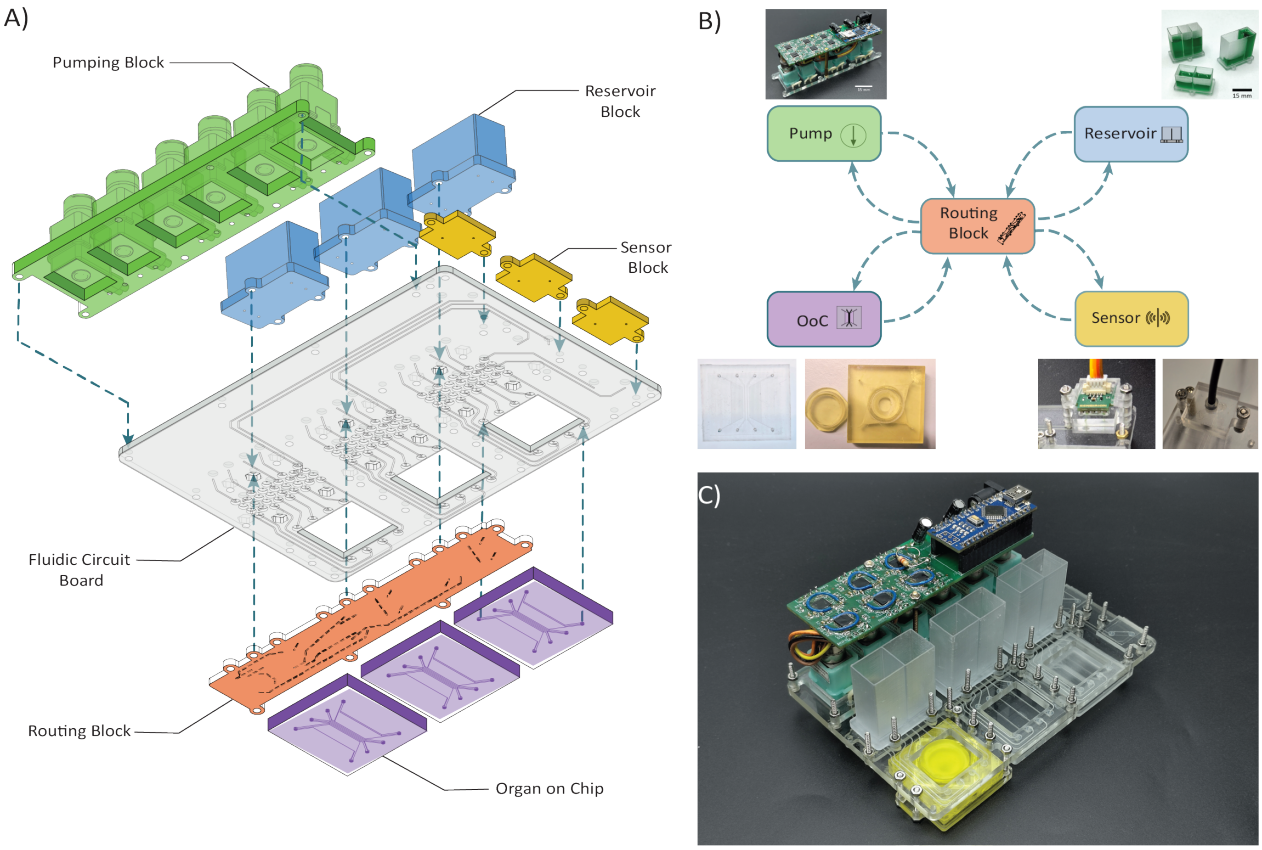

Figure 1: Overview of the Starterkit by A. Paul (unpublished). A) An exploded view of the components that make up the Starterkit. B) A schematic overview of how the different components are connected. C) A picture of the assembled Starterkit.

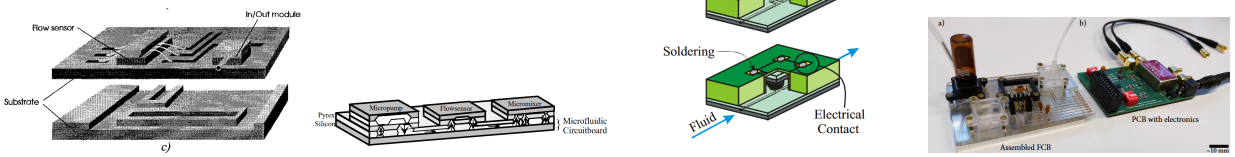

(a) Exploded view of the modular concept by Lammerink *et al.* [9].

(b) More standardized pyrex-silicon sandwich solution by Schabmueller *et al.* [10].

(c) PCB attached sensors, MATAS platform, by Gilde *et al.* [11].

(d) Modular coulter counter by Dekker [12].

Figure 2: From left to right a quick history of modular microfluidic platforms.

2 Background

2.1 State of Modular Microfluidics

The microfluidic field has already started playing with modular concepts, starting in the 1990s. First, the idea of combining sensors and fluidics in one chip was proposed with the micro total analysis system by Manz *et al.* [8]. After this, the concept quickly gained traction, and already a modular system was proposed by Lammerink *et al.* [9]. They proposed a system where modules would be bonded using existing bonding techniques to a substrate with the fluidic channel network called the Channel Circuit Board. This design was further worked out by Schabmueller *et al.* [10] in 1999 to use pyrex-silicon sandwich material so only anodic bonding would be used for attaching the modules. While these solutions were modular, the modules would be attached permanently, and they would not be reusable. In 2005 Gilde *et al.* [11] proposed a new solution they called 'MATAS', Modular Assembly Technology for micro Analysis/synthesis Systems, where the sensors were pushed on the channel network, now called Fluidic Circuit Board (FCB), and held in place by solder in a bigger Printed Circuit Board (PCB). This solution favored small sensors and showed an interest in developing modular microfluidic platforms by companies.

Due to the high rise in interest in microfluidic systems but the lack of consistency in their fabrication and use, a consortium for Microfluidic Manufacturing set up an ISO workshop in 2016 to start developing a microfluidic standard[7]. The idea is that this would increase the ease of use of microfluidic platforms in research by easily combining modules from different manufacturers to suit the application's needs[12]. The usability of this standard was demonstrated by Dekker *et al.* [13] by making a modular coulter-counter that was interconnected through an FCB.

The ISO 22916:2022 standard[15] following this workshop outlines how to interconnect different modules. The basis is to fit all modular fluidic building blocks (MFBBs) inside the size of a 96 wells multiplate. A framework is laid out on which modules can be built by defining the reference points, dimensions, port pitch, and exclusion zones. An example of how the standard can be applied can be seen in Figure 3. The standard is aimed at the whole field of microfluidics and is, therefore, rather general. How the clamping and sealing of the connections is done is not explicitly stated in the ISO documentation and is left to the developer of a module. To show the potential of the standard for organ-on-chip applications and to advocate its use, a Starterkit is being developed that also tries to fill in the unknowns of the ISO standard. The goal of the Starterkit is to have as much as possible integrated and contained within the Starterkit dimensions such that the least amount of cables and external devices are needed to run the platform and its experiments. This is specifically useful for the target organ-on-chip applications since the devices need to fit in an environmentally controlled chamber. The Starterkit strives to be open and accessible. Therefore, researchers can add their modules to the platform. While all these integrations increase the complexity of the platform, they should not compromise the platform's ease of use.

Shown in Figure 1 A, the basis of the Starterkit consists of a pump module with six peristaltic pumps, which can be controlled individually, and three reservoir blocks in the middle with each two reservoirs. Three microfluidic building blocks (MFBBs) of 30 x 30 mm are designed to be swapped for functional blocks, such as a chamber for cell cultures. On the side, there is room for three 15 x 15 mm MFBBs, which can be connected to measurement setups to do measurements of the fluids inside the channels. Everything is connected by the FCB, which has a fully customizable routing block, so the layout of the connections can be changed per application as shown in B. For now, the measurements carried out on the processes on the board are done with external devices.

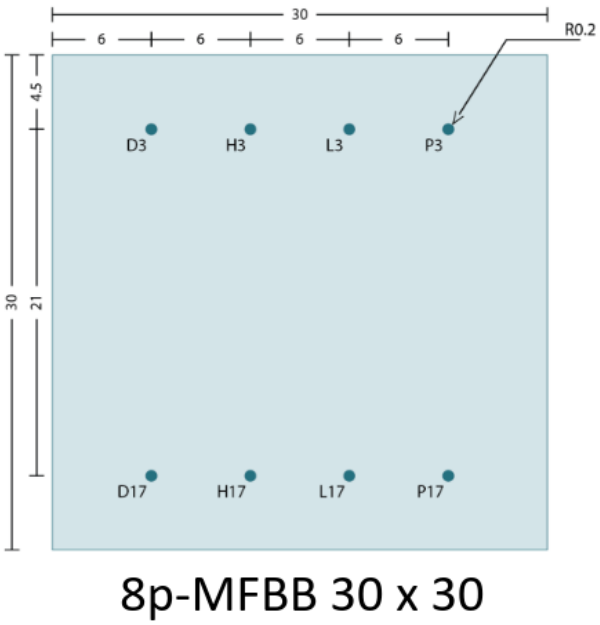

Figure 3: Example application of the ISO standard on Modular Fluidic Building Blocks for the growth of cell tissues by Safai [14] as used in the Translational OoC Platform Project and the Starterkit. (units: mm)

2.2 Monitoring Organ-on-Chip

An Organ-on-Chip (OoC) is a microfluidic platform with cell cultures to mimic the functions of a human organ[16]. At the center of an OoC system is the tissue to be studied. This cell culture has to be monitored to keep it in good condition and to measure the effects of tests done. Since the environment around the cells is a very good indicator of how the culture itself is functioning, a feasible solution can be to not look at the cells directly but the environment around them for continuous monitoring. Environmental variables like pH, oxygen and/or carbon dioxide concentrations, and the presence of specific ions are essential for the viability of the culture. Electrical sensors are the preferred way of monitoring these kinds of variables in OoCs due to their simplicity and the field's maturity in micro-electronics and electrodes[16].

pH can, for instance, be measured by use of an Ion-Sensitive Field Effect Transistor (ISFET)[17] or Ion-Sensitive Metal Oxide electrode[18]. Both of these techniques rely on measuring a change in potential. The Nernst equation governs the signal measured and can reach a maximum resolution of 59 mV/pH[19], and a common resolution is around 46 mV/pH[20].

Oxygen concentration is more easily measured by its diffusion to inert electrodes. The main problem is that these kinds of sensors consume the dissolved oxygen in the solution. These sensors measure a change in conducting current to the electrode with resolutions up to a couple of nA per mg/L oxygen[21].

Specific ion concentrations can be determined using electrodes coated in ionophores, which change their charge based on ion concentration in the solution[22]. Again, the response of these electrodes is governed by the Nernst potential. This means that when measuring ranges of ion concentrations in human serum, the potential change is about 9.5 mV for a change in K^+ concentration from 3.5 to 5.0 mM[23].

To inspect the integrity of cell layers, the potential drop across a barrier of cells can be measured. At a fixed or sweeping frequency, the layer's electrical resistance can, therefore, be determined. The technique used for this kind of measurement is Electrical Impedance Spectroscopy, and the typical frequencies range from 10 Hz to 100 kHz but sometimes go up to 1 MHz[24]. The impedance can be monitored over time and give information about the development of the cell layer. These Trans Epithelial Electrical Resistance (TEER) measurements are important in, for instance, intestinal epithelium cell cultures[25].

2.3 Electrochemistry

The electronic sensors used in OoCs are often based on electrochemical principles. The mechanisms of the measurements can be divided into non-faradaic and faradaic measurements. With non-faradaic, there

Table 1: Overview of specifications of commonly used sensors in Organ on Chip applications.

Variable	Expected output	Expected input
pH sensing	Change in potential; 46-59 mV/pH [17][20]	negative bias voltage for ISFET
Oxygen concentration	nA current change	-0.7 V potential supply[26]
Ion concentration	changes in a couple of mV[23]	No input, measure OCP
TEER	1-100 kHz, amplitude ~10 μA [24][25]	Excitation potential 1-100 kHz 10 mV amplitude

is no charge transfer from the electrode to the analyte. Instead, a double-layer capacitance is formed on the surface of the electrode, which is consequently charged and discharged. These measurements with an alternating current are called Electrical Impedance Spectroscopy (EIS). In principle, this method only requires two electrodes, a Working Electrode (WE) and a Counter Electrode (CE) in non-faradaic situations[27]. An electronic equivalent circuit can be derived when sweeping the frequency and measuring the current response. A Randles circuit is the basic electronic equivalent circuit that describes an electrochemical cell. This circuit describes the impedance of the solution and the electrode-electrolyte interface[28]. This interface consists of a double-layer capacitance and the charge transfer resistance, as seen in Figure 4.

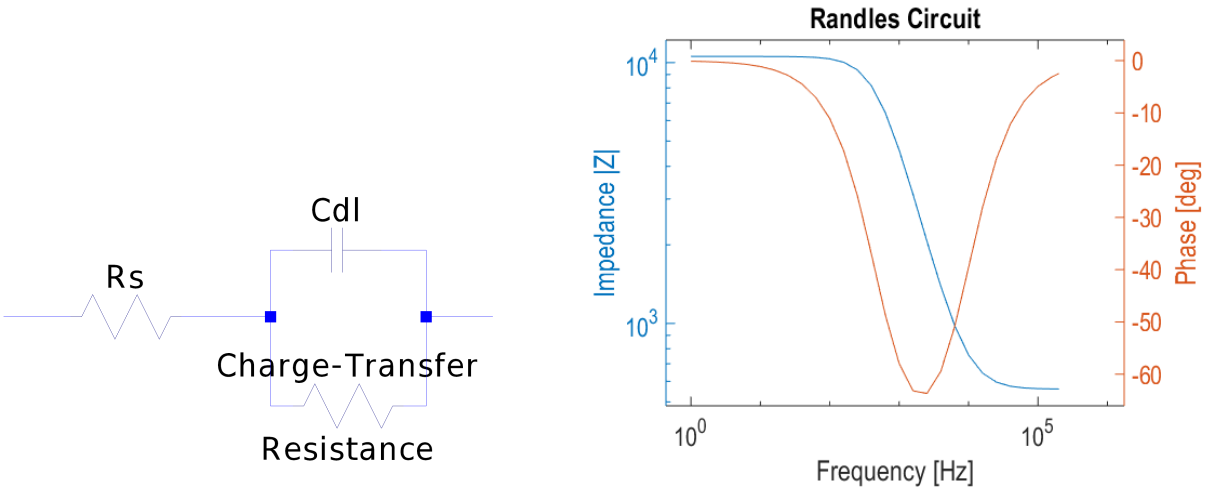

Figure 4: The Randles Circuit and its simulated typical response to an AC signal sweep. For the simulation Rs = 560 Ω, Cdl = 33 nF and Charge transfer resistance = 10 kΩ.

Faradaic measurements, on the other hand, have at their basis measuring reactions that release electrons to or consume electrons from an electrode. This can be measured as a change in the electrode's potential or a current of electrons flowing to sustain the chemical reaction. This means the reaction kinetics are measured and need to be taken into account[29]. Faradaic measurements, in turn, can be split up into potentiometric and amperometric measurements. For potentiometric measurements, a change in potential between electrodes is measured. Measuring the Open Circuit Potential (OCP) is potentiometric since it does not apply a potential to the electrodes and measures the resting potential at the electrodes. To have a reference at which these potentials are measured, a third Reference Electrode (RE) has to be added to the Working and Counter Electrode. The measured resting potential is caused by the rate of oxidation and reduction reactions on the electrode surface when no current is flowing. This means that the OCP gives information about the ratio between redox species in a solution and can give information about the concentration of the species[30].

With amperometric measurements, the current is measured by applying a voltage. Cyclic Voltammetry (CV) is an example where a sweeping voltage is applied, and the current response of the analyte is measured[30]. This response is proportionate to the chemical reaction at the electrode and follows the Randles-Sevcik Equation:

$$i_p = 0.4463nFAC\left(\frac{nFvD_o}{RT}\right)^{\frac{1}{2}} \quad (1)$$

Where the peak current (i_p), the difference before the peak starts and the highest point, will linearly increase with the square root of the scan rate (v) and is dependent on the number of electrons transferred during the reaction (n), the Faraday constant (F), the area of the electrode (A), the bulk concentration of the analyte (C), the diffusion coefficient of the oxidized analyte (D_o), the temperature in Kelvin (T) and the gas constant

(R). Following equation 1, the current response depends on the concentration and the scan rate when the environment stays the same. An example of such a measurement has been carried out. It can be seen in Figure 5 where the peaks in the graph represent the potentials at which the oxidation (higher potential of the two) or reduction (lower potential) takes place. When more redox couples are present in the solution, more peaks can be seen in the graph, indicating their reduction and/or oxidation potentials. These peaks can, in turn, be used to identify the redox species in the solution.

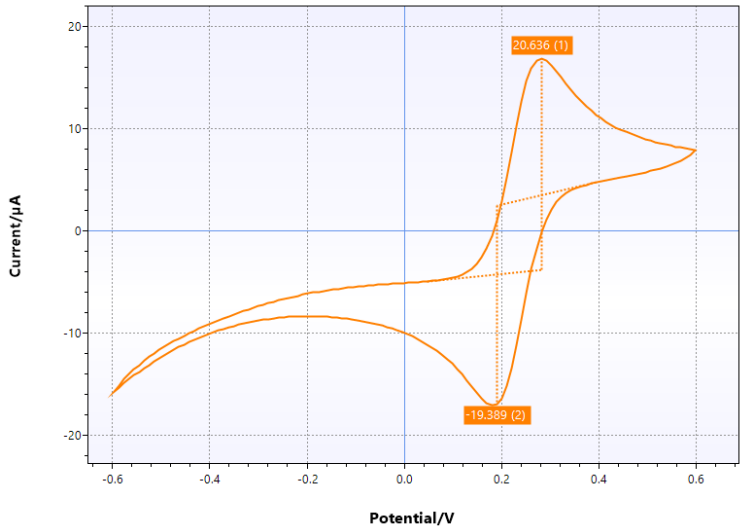

Figure 5: Cyclic Voltammetry measurement of a solution of 100mM ferrocyanide at a scan rate of 100 mV/s. The peaks of the oxidation and reduction reactions are visible.

Chronoamperometry (CA) is also a form of an amperometric measurement. Here, a constant potential is applied for a certain amount of time, and the current over time is measured[31]. The Cottrell Equation describes this reaction:

$$i = \frac{nFAC_0\sqrt{D}}{\sqrt{\pi t}} = XC_0\frac{1}{\sqrt{t}} \tag{2}$$

Where the current (i) is proportionate to the square root of time and the initial concentration (C_0), here D is the diffusion coefficient of the species. When this equation is simplified, there is a linear relation between the current and the $\frac{1}{\sqrt{t}}$ when all other parameters stay the same. The slope of the graph changes proportionally with a change in concentration, as can be seen when simplified by putting the constant variables in X. Thus, it can be used to determine proportional concentration change if all other variables are unknown but constant.

3 Design

3.1 Requirements

As described in the background, the ISO standard aims to make it easier to interconnect microfluidic modules and, therefore, make microfluidics more available. The Starterkit's vision adds to that by aiming for a fully standalone OoC platform that is easy to use. The platform should be modifiable to be used in many different situations. Currently, the integration is mainly focused on the microfluidic side of the platform. The vision for electronic integration on the platform is to make it as modular as the microfluidics, to be robust to work in the electrically noisy environment of the Starterkit itself and the setups around it, to use open standards and common components, and to be easy to implement by an end-user. These visions can be further specified into concrete requirements, which are summed up in Table 2.

First of all, the device needs to fit on the Starterkit and not interfere with the standards already set by ISO. It is desirable to only take up the space of one culture chamber so as not to interfere with the connections present. Therefore, the device should fit in the same area as a 30 x 30 mm MFBB. This way it can be placed on top or below the chamber. When the device is close to the MFBB, the connections to the sensor can be as short as possible, which can increase the signal quality since the wires for the analog signals will be short and, therefore, pick up less electrical noise from the environment. A digital communication protocol should be used to have minimal noise in the communication to and from the module. Since the primary use of the Starterkit will be in environmental chambers for the cell cultures, the cables used by the module should be minimized. Therefore, only one cable will transfer data and/or power. To continue the vision of the ISO standard and the Starterkit, the solution should be modular and independent from the microfluidic module used. This means the device must be easily attached to the Starterkit and easily removable. Using the existing hardware of a 30x30 mm MFBB is desirable, and electrodes should be attached to the device in a non-permanent and reusable way.

The goal of the device is to monitor the cell cultures. Section 2.2 explains parameters that are important to measure. Here, it is indicated that there are different methods to measure these parameters, and the measurement techniques depend on the kind of electrodes or coatings. There is a set of techniques that encompass most of the measurements that the device should be able to do. First, Electrical Impedance Spectroscopy is used to do TEER measurements to measure changes in the cell layer. From this, stresses and thickness in the cell layer can be derived. Second, Cyclic Voltammetry is important to see the oxidation and reduction potentials of species inside the solution. Lastly, chronoamperometry is important in determining the concentrations of analytes.

The target audience for this device is researchers who want a plug-and-play product. In that way, the device needs to interface with already existing peripherals like a computer. It needs good documentation, and it should be easy to perform the measurements. The device must also be adaptable to be modified to fit the users' needs. Using common components and standard fabrication techniques should help with that requirement.

Table 2: Overview of the requirements for the design of the device.

Goal	Requirement
Fit on the Starterkit	Not interfere with the existing connections Only take up as much space as a 30x30 mm MFBB
Low electrical interference	Keep electrode connections short Use a digital communication protocol
Few external connections	Use one cable for communication and/or power
Modular device	Use existing mounting hardware Electrodes are attached in a non-permanent way
Monitoring cell cultures	Provide electrical impedance spectroscopy, cyclic voltammetry and chronoamperometry measurement techniques
Plug-and-Play	Interface directly with a computer Have a usable interface and good documentation
Adaptable	Use accessible components and fabrication techniques

3.2 Measurement Circuit

Specific electronic requirements can be derived from the electrochemical measurement techniques mentioned in the previous section and section 2.2. For EIS measurements, frequencies need to be generated. Looking at TEER measurements, the frequencies generated must be at least from 1 Hz to 100 kHz with a variable amplitude between 1 and 100 mV[24]. These frequencies also need to be measured and will have amplitudes in the µA range. To be able to do CV measurements a sweeping potential should be applied in a range of at least -1 V to 1 V. On the other hand, currents should be measured with a resolution of a couple nA[30]. Looking at CA measurements constant potentials should be applied between -1 V and 1 V. The current measurements for this technique should be more precise with a resolution in the tens of pA[26].

Looking at these electrical requirements, a reliable voltage source that can provide the DC and AC signals and a way of measuring potentials and currents is needed. The ranges to measure are very broad, so variable amplification of the electronic signals is needed. Since the currents are low, low-noise amplification is also needed. The EIS frequencies to be measured also ask for fast measuring.

The first choice was made on the measurement circuitry. Since it needed to fit on a specific 30 x 30 mm footprint, a custom solution had to be made. The research was done on making the device from scratch by looking for a suitable microcontroller that could be paired with available integrated circuits to get the functionality desired. If only looking at EIS circuitry, circuits for wearables have been reported that could produce and read signals up to 100 kHz[32]. There are also commercially available spectroscopy chips meant for radio analysis that could be used. Since the device should measure more than just the impedance spectrum, the complexity rises quickly by adding abilities for these circuits to measure low currents for chronoamperometry. Furthermore, these circuits would have had to rely on self-written programs and firmware to function. This increases the project's complexity even more and decreases the ease of use for an end-user since support is not guaranteed. If the circuit had been purpose-built, this would have decreased compatibility with test protocols other than the proof of concept tests designed.

Looking at commercial potentiostats used in labs, most are bigger than the footprint specified, like the Bio-Logic SP-300 which is 20 by 40 cm. Smaller portable potentiostats do exist from the likes of MetrOhm and PalmSens, but not down to the footprint desired. PalmSens has an OEM product, the EmStat Pico, that is developed together with Analog Devices. This module is 18 x 30 mm and, therefore, should fit inside the 30 x 30 mm footprint. Since this is an OEM product, all peripherals around can be designed separately to suit the requirements of this project. The downside of being a commercial product is that the manufacturer's specifications cannot be modified. A selection of these specifications is shown in Table 3 and does fit the requirements set earlier in this section. The positive of being a commercial product is that it has extensive documentation and a compatible analysis program to do the measurements.

Table 3: Selection of EmStat Pico module specifications[33].

Element	Specification
Communication	UART (to module), I2C and SPI (to peripherals)
DC-potential Range	-1.7 to +2 V
Acquisition Rate	1000 datapoints/s
Potential Resolution	56 uV
Max. Current Resolution	5.5 pA
DC-potential Source Resolution	395 uV
EIS Frequency Range	0.016 Hz to 200 kHz
AC-amplitude Range	0.708 V peak-peak
Amplifier input	>1 TOhm // 10 pF
Storage	4000 datapoints
Size	18 x 30 x 2.6 mm
Interface	PSTrace, MethodScript

3.3 Electrodes

A stable reference electrode must be used for the proof of concept measurements. Common reference electrodes are the standard hydrogen electrode and potassium chloride (KCl) saturated silver/silver chloride (Ag/AgCl) electrode. The standard hydrogen electrode is hardly used in common testing since it is impractical, and both reference electrodes cannot be manufactured to be small enough to fit inside a microfluidic

chip[34]. A quasi-reference electrode can be made from silver by depositing a silver chloride layer to make a quasi-reference Ag/AgCl electrode. If there is potassium chloride or sodium chloride inside the solution this electrode should give a stable reference potential. Luckily these salts are important for cells to function and are therefore present inside most biocompatible solutions like Phosphate Buffered Saline (PBS). For EIS measurements, the only requirement is to have inert working and counter electrodes where no reactions take place with an open circuit. Platinum and carbon electrodes are often used in this case[28]. In conjunction with the quasi-reference electrode, platinum can also be used to measure the reduction of oxygen and, therefore, oxygen concentrations with chronoamperometry[26]. Cyclic Voltammetry can also use the platinum electrodes when measuring oxidation and reduction reactions when the redox pairs of the species are in solution[30].

3.4 PCB design

To fit on the Starterkit and design for a one-cable setup, the circuit components must be fitted on a printed circuit board (PCB). It was chosen to dedicate one side of the PCB fully for the EmStat Pico module since it is the most significant component to be used and the PCB may not be much bigger than the module itself to still fit in the same footprint as a 30 x 30 mm MFBB. Since margins for solder pads of the EmStat Pico module were needed, the PCB is a little wider than 30 mm, as can be seen in Figure 6. To be mechanically compatible with the Starterkit and easy to attach to the platform, the PCB is designed to have holes that line up with the mounting screws for the clamp of the MFBB.

Since the EmStat Pico communicates to a computer with the UART protocol a conversion from UART to USB is needed to have one cable running from the Starterkit and be directly compatible with a computer. UART to USB conversion on the PCB has been chosen to minimize the external devices needed. A USB-C connector was considered, but due to the complexity of the connector and the USB-C standard, there was a higher chance of it not working in different setups. Therefore, the USB connector chosen is a micro-USB connector since this is a versatile connector that has a small footprint and is foolproof in its standard for connecting to a computer. In the layout of the PCB, the power and UART pins of the EmStat Pico were also exposed directly via headers. This way, if the conversion to USB is not desired direct UART communication is still possible. It is also possible this way to connect a potential Bluetooth module such that controlling the device can be done wirelessly if 5 V power is provided to the device via its exposed pins. Another feature of the PCB is the inclusion of two microswitches. These switches are there to internally connect CE and RE since this is desirable in some situations where only two electrodes are used. This removes the need to bridge the contacts of the connector, which makes the device more user-friendly.

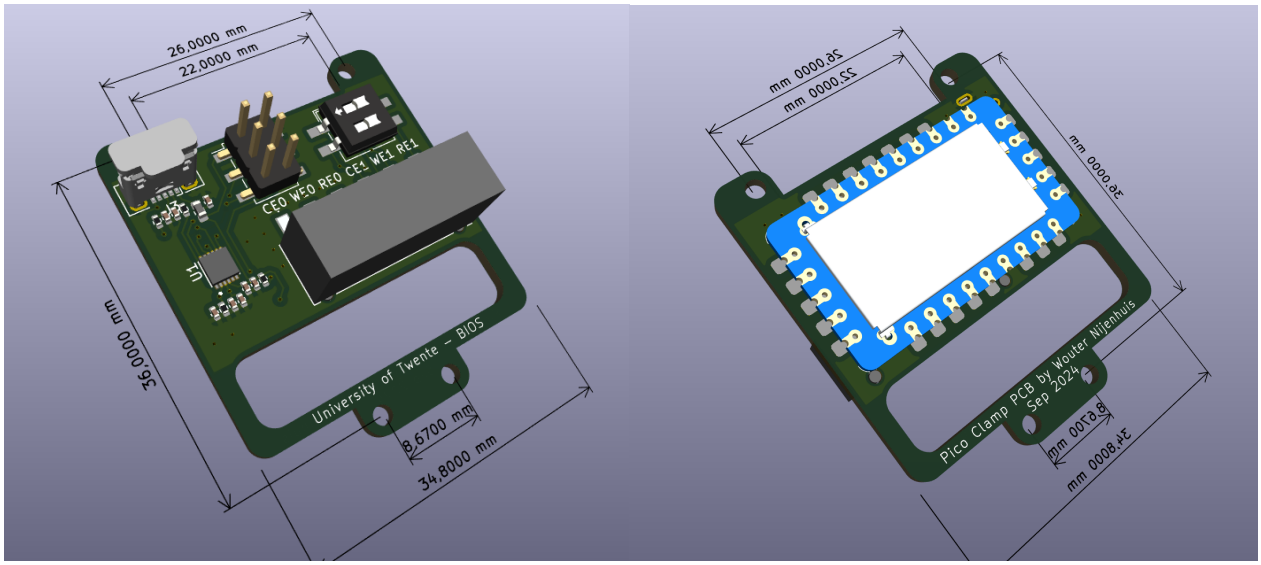

Figure 6: 3D model of the proposed PCB design. The mounting holes line up with the screws for MFBB attachment and the hole in the PCB is for electrodes to pass through to the clamp on the top side. The EmStat Pico Module occupies the whole board on the back.

One of the more important aspects of the PCB is the way the electrodes of the MFBB are connected to the device since this needs to be non-permanent and reusable. Multiple connector candidates were considered, as seen in Figure 7. Starting with high-frequency connectors that are often used for Wifi or Bluetooth anten-

nas. The connectors are small and would fit the design, but a lot of modification of the electrodes is needed to fit them with the correct connectors to attach to the device. This would have decreased its ease of use and versatility. Ribbon cable connectors were considered as well. These connectors are used to connect flexible PCBs or flat ribbon cables to a rigid PCB. This would limit the use of the device to screen-printed electrodes. Therefore clamping connectors were considered. Push-in clamping connectors are attractive due to their ease of use, when pushing in a wire the clamp shuts and keeps clamping pressure on the wire. The drawback of this system is that with small electrode wires, the push-in connectors do not hold onto the wires. If the wires are fragile, they could even break inside the connector. So, bigger screw terminal-type clamping connectors were chosen. With these connectors, the clamping pressure can be chosen while screwing in the electrodes. Thus, care can be taken with fragile wires. Next to that screen-printed electrodes can still be used if they are designed with conductive fingers to fit exactly in the screw terminals.

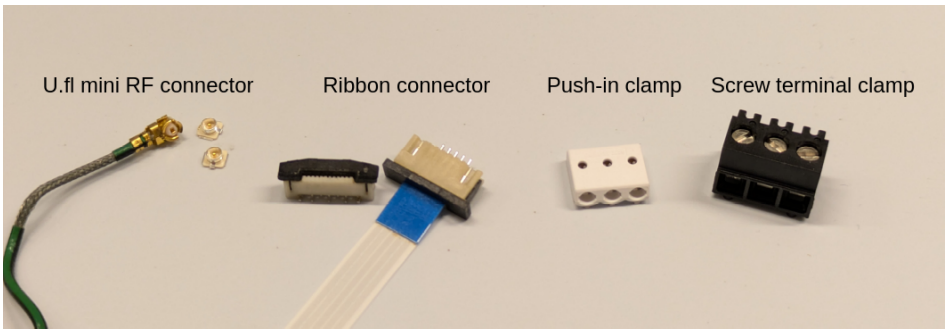

Figure 7: The different types of connectors considered

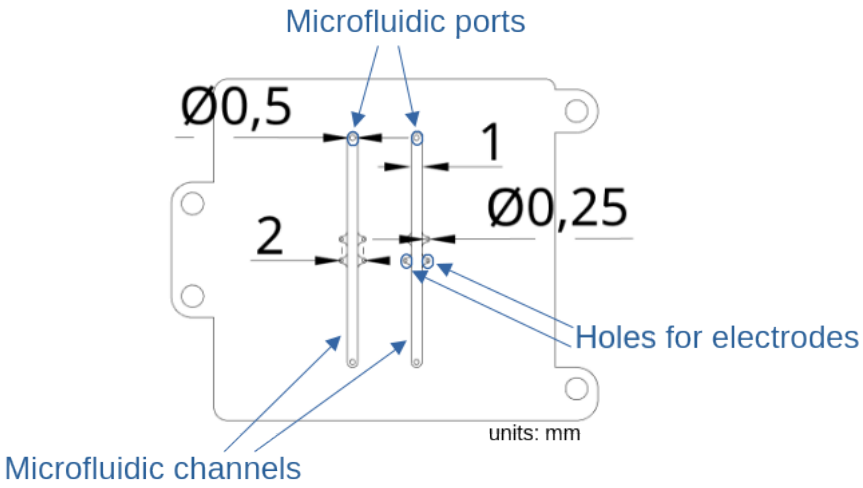

Figure 8: Drawing of the design for the channels in the MFBB.

3.5 MFBB

The design of the MFBB can be kept fairly simple. For the proof of concept measurements only the electrode wires need to be held in place with the possibility of a solution flowing in between them. The most important part of the MFBB is that the in- and outlet ports will fit the Starterkit standard. Since the EmStat Pico has two measurement channels also two separate flow channels are designed in the chip. Each channel has a place for four electrodes so their position can be chosen freely, and the exposed holes can be covered with glue to close the channels. The channel design is made so that with a hole through the back, it can be used with stick-in wire electrodes, and the front of the channels can be closed off with a flat cover piece. If the holes are not made in the back, the cover can be swapped for a screen-printed electrode, and the design of the channels does not have to be altered. To prevent the electrodes from being too close to each other, the channel is made 1 mm wide, such that the center of the electrodes opposite of each other are 2 mm apart, and diagonally, the electrodes are 2.8 mm apart. The channel is milled out of PMMA to be easy to work with and stiff enough to be clamped easily. The channels are made 400 microns deep which means the electrodes sticking in the MFBB are also in contact with the solution for a length of 400 microns.

4 Methods

4.1 Fabrication

The device's circuit diagram (Appendix C) and PCB layout were made in KiCAD 8.0. Care was taken to keep the design as small as possible and to keep a place for electrodes to go through so as not to exceed the 30 x 30 mm dimensions too much. The PCB was manufactured by Eurocircuits. The component choices were made using the parts' availability in the LCSC database. This way, the PCB could possibly later be ordered and fully assembled (except for the EmStat Pico module) by a third party, JLCPCB. For this project the components were ordered separately and soldered on by hand. The drawings for the MFBB were made in Onshape and milled out in a sheet of 2 mm PMMA using a micro-mill. The electrodes were glued in using Norland Optical Adhesive 68, a UV-curable glue with a high viscosity so it would not seep into and clog the channel. The cover was stuck on using double-sided tape.

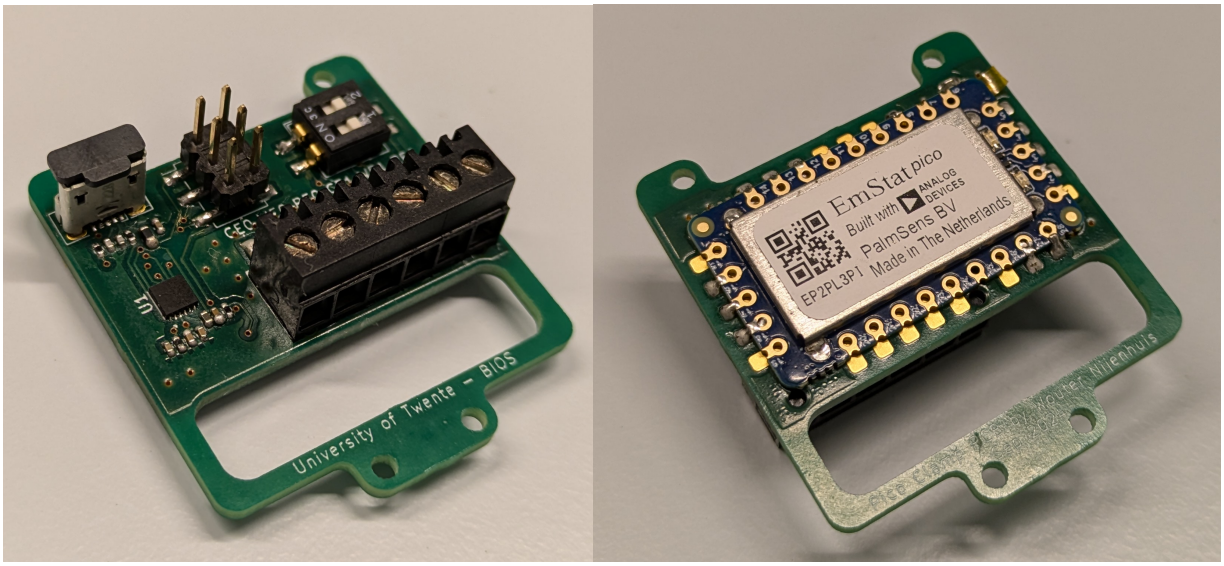

Figure 9: The front and back sides of the produced PCB with all the soldered components.

A couple of experiments are designed and described down below to measure the design's feasibility. These experiments show whether the design produces data that can be used in Organ-on-Chip applications and test its capabilities in common scenarios.

4.2 Comparison to Biologic

A crucial step is to look at impedance spectroscopy due to handling high frequencies and parasitic elements in the wires and the circuits. The EmStat Pico development board is compared against an SP-300 Potentiostat from BioLogic. Test boxes are used to compare the exact same parameters. These test boxes are electronic circuits that mimic the electrical equivalent of an electrochemical cell. The electronic circuits of these reference cells are shown in Figure 10. For a comparison to a theoretical response curve the test circuits are also simulated in LTspice.

The signal used during the Electrical Impedance Spectroscopy is an AC signal of 10 mV in the range of 1 Hz to 200 kHz. With 6 measurements per decade, this gives 32 data points per measurement.

4.3 Preparing Electrodes

The solutions' measurements are performed using a three-electrode setup consisting of two platinum electrodes and one quasi-reference Ag/AgCl electrode. The platinum electrodes are cut from a larger spool of platinum to appropriate lengths and cleaned with DI water before use.

To fabricate the quasi-reference Ag/AgCl electrode a protocol is used as described by Bossink [26]. The protocol is extrapolated to be used with bigger silver surface areas. Silver wire of 203 µm in diameter is placed in 1 M KCl, and with a platinum counter and reference electrode, a constant current is applied using

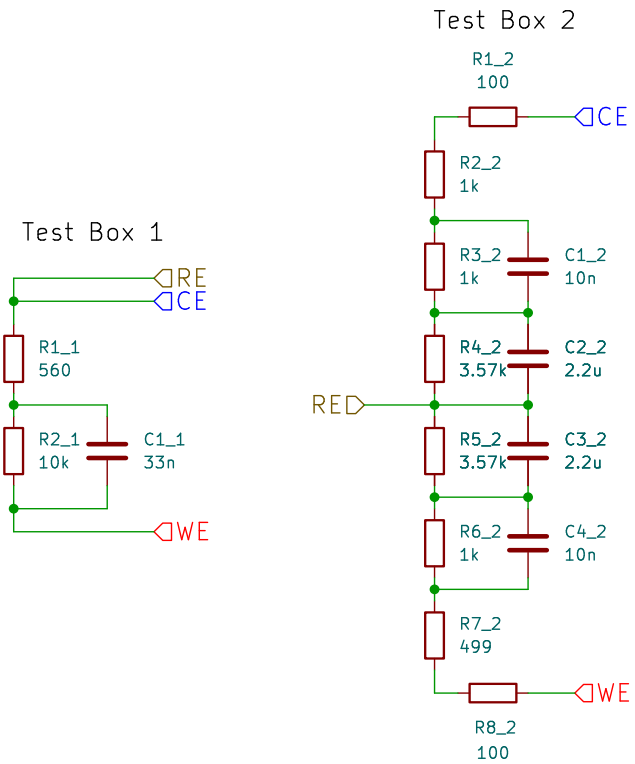

Figure 10: The electric circuits of the Test Boxes used in the comparison of the EmStat Pico development board to the BioLogic SP-300 and LTspice simulations.

the BioLogic SP-300. This current is dependent on the surface area of the electrode and can be found in Table 4. This current is applied for one hour after which the AgCl layer thickness can be calculated using the amount of coulombs transferred.

The stability of the electrode is tested by measuring the open circuit potential against a reference saturated Ag/AgCl electrode for one hour, the results of which can be found in Appendix A.

Table 4: Showing the current applied for the electrode lengths in the 1M KCl solution and an approximation of the AgCl layer thickness that will be deposited.

Electrode length [cm]	Current applied [µA]	Deposited mass [g]	Approximate AgCl layer thickness [µm]
1	0.0574	3.094e-4	8.638
2	0.1150	6.169e-4	8.655

4.4 Impedance Spectroscopy

To see how the impedance spectroscopy of the developed EmStat Pico PCB behaves it is tested on KCl solutions of different concentrations. The KCl solutions are prepared by diluting a 1 M KCl solution with DI water. The resistivity of the different concentrations is measured using a S47 SevenMulti™ from Mettler Toledo, and the fluid's resistance is calculated by dividing it by the distance between WE and RE. As per the design, the electrodes are put in the fluidic chip designed such that 0.4 mm of every electrode is in contact with the solution. The counter and working electrode are 2 mm apart, the reference electrode is located 2.8 mm from the working electrode. The microfluidic chip is put on a tester board so the solutions can be pushed through the channel with a pipette, the setup can be seen in Figure 11. The electric signal is applied at DC 0 V to Open Circuit Potential (OCP) with an AC component of 25 mV. The signal sweeps from 200 kHz to 1 Hz with 7 data points per decade for 38 data points per measurement.

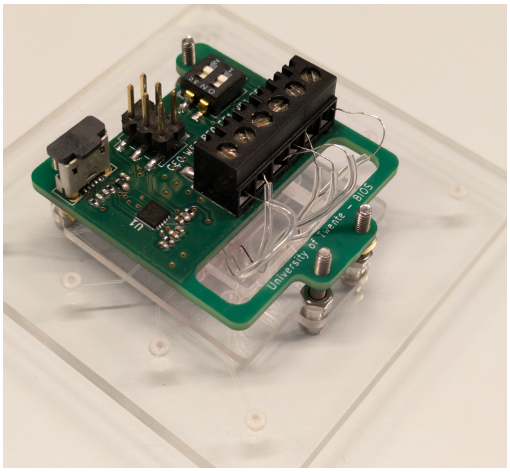

Figure 11: The EmstatPico device on the tester board. On the sides of the translucent tester board, o-rings can be seen, which correspond to the in/outlets of the MFBB attached to the underside.

4.5 Cyclic Voltammetry

Cyclic Voltammetry is performed with the three-electrode setup in the microfluidic chip, as mentioned before, but now the chip is also put in the Starterkit so a controlled flow of fluid through the chip can be realized. A way of adding a gas flow through a solution in the reservoir is made, as seen in Figure 12. The amount of oxygen in Phosphate Buffered Saline (PBS) can be controlled by using a Bronkhorst IQ+FLOW mass flow controller connected to a pure nitrogen line and a line of atmospheric air. The gas flow is kept constant at 100 sccm while varying the ratio of nitrogen and air. Before the measurements start, the air is bubbled through the PBS while the fluid is pumped around the fluidic channels at 25 µL/min for 2.5 hours. After which 100% nitrogen is bubbled through the PBS, and the CV measurement is done six times at a 10-minute interval, still with a fluid flow of 25 µL/min. The CV begins at 0 V to OCP and has the first vertex at -800 mV and the second vertex at 300 mV. The scan rate is set to 100 mV/s with two scans per measurement where the second scan is taken as the data to be analyzed.

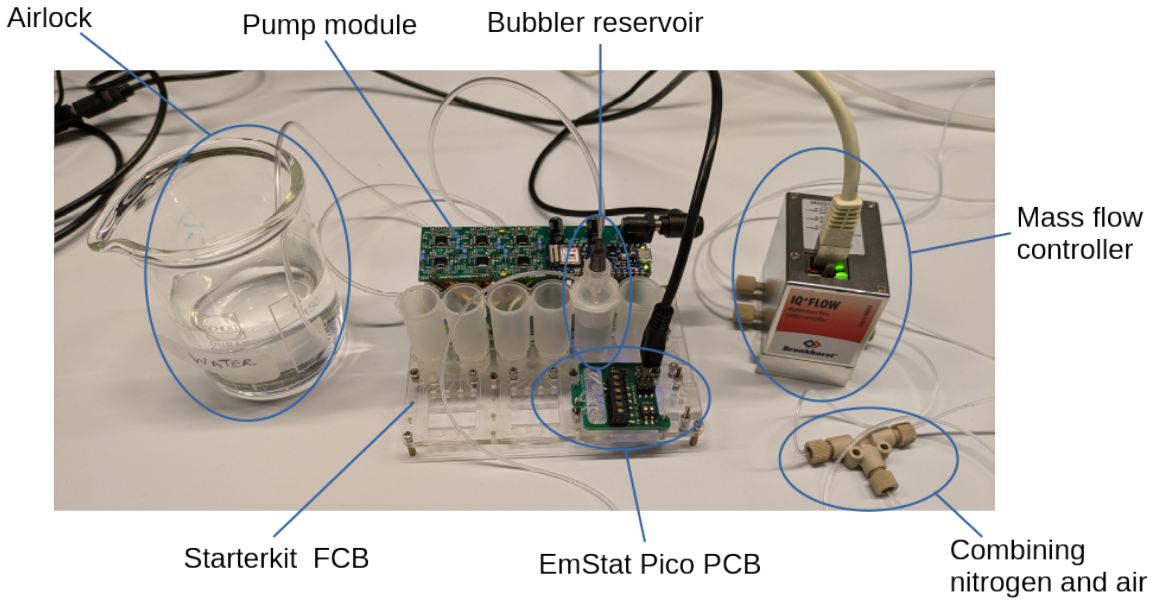

Figure 12: The setup used for flowing gas through the PBS. The Bronkhorst mass flow controller is on the right and feeds the gas through the reservoir of the Starterkit in the middle. The Starterkit circulates the PBS through the microfluidic chip. An outlet of the reservoir is put into a beaker with water to counter any gas flow from outside. The EmStat Pico PCB is positioned above the microfluidic chip.

4.6 Amperometry

The amperometry is performed in the same setup as the CV. Again, the gas flow is kept constant at 100 sccm and the fluid flow at 25 µL/min, but now the ratio of nitrogen and air is varied. Before the measurements, 100% nitrogen is bubbled through the PBS for 2.5 hours. The ratios of nitrogen to air taken are 4/0, 3/1, 2/2, 1/3, and 0/4. After every measurement, the ratio of gasses is changed and flows through the PBS for 30 minutes before the next measurement is taken. The current flowing through the working electrode is measured for 5 seconds with a sample rate of 10 ms at an applied potential of -700 mV, the reduction potential of oxygen.

5 Results

5.1 Comparison

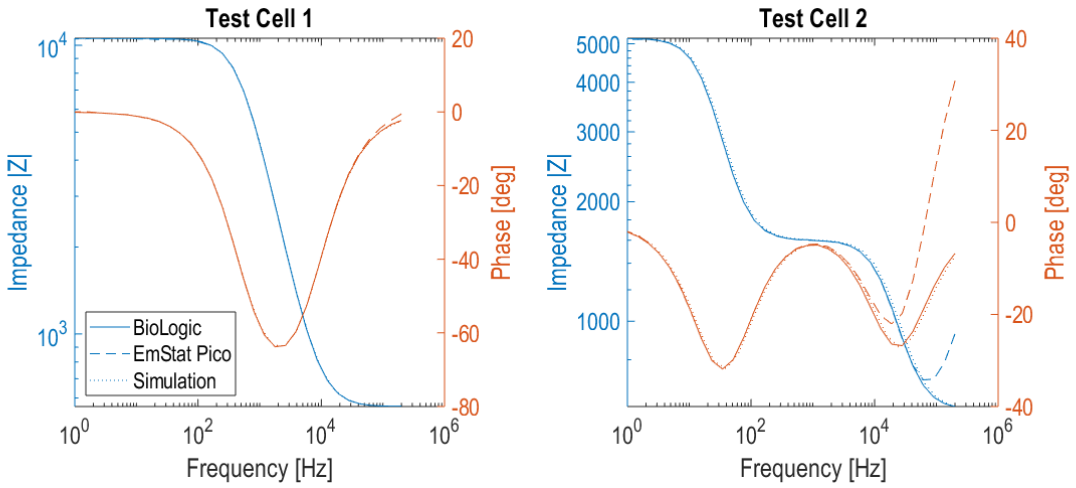

Figure 13: Comparison results between a BioLogic SP-300, EmStat Pico development platform, and LTspice Simulation of impedance spectroscopy measured on test circuits. In blue is the absolute value of the complex impedance, and in orange is the phase of the signal. The BioLogic and Simulation results are almost equal, so the lines are overlapping.

Figure 13 shows impedance spectroscopy on two test circuits. The measurements of the EmStat Pico development platform show great similarity with the BioLogic used as standard and the simulations done in LTspice. The biggest difference is seen at higher frequencies where most capacitance is ignored in the measurements, and only resistances are measured. The impedance measured by the EmStat pico curves up again, which indicates that inductance is measured at those frequencies, which is not present in the other measurement methods.

5.2 Impedance Spectroscopy

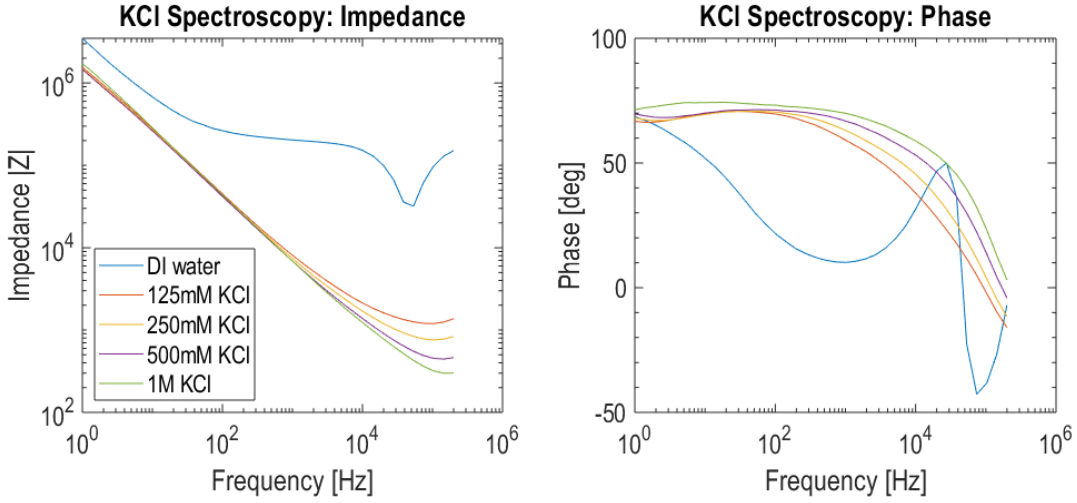

Figure 14: Electrical impedance spectroscopy of different concentrations KCl from 1 Hz to 200 kHz. The frequency response resembles the response that is expected from a Randles circuit. The impedance at higher frequencies diverges and there is a clear distinction in impedance between the different concentrations.

Figure 14 shows the impedance spectroscopy done at different concentrations of KCl. The response is comparable with the response to a Randles circuit, as expected, with a higher impedance at low frequencies where the double-layer capacitance is dominant. There is a clear difference seen in resistance at higher frequencies where the double-layer capacitance is negligible, and only the resistances of the electrochemical cell are measured.

In a log-log plot, a linear relation is expected between the concentration and the measured impedance following the equation $R = \rho C$, where R is the electrolyte resistance, ρ is the resistivity of the electrolyte, and C is the electrochemical cell constant. Since the exact electrochemical cell constant of this setup is hard to determine to use in calculating the expected measured impedance, the real impedance measured is compared to the resistance of the different solutions in Figure 15 and Table 5. It becomes clear that the linear relation is as expected, but the real impedance measured is an order of magnitude higher than the resistance derived from the resistivity of the KCl solution. The calculation of the theoretical resistance of the fluid is done by taking the molar conductivity of KCl of 149.9 Scm²/mol, multiplying that by the concentration, and multiplying the inverse with the distance between the RE and WE.

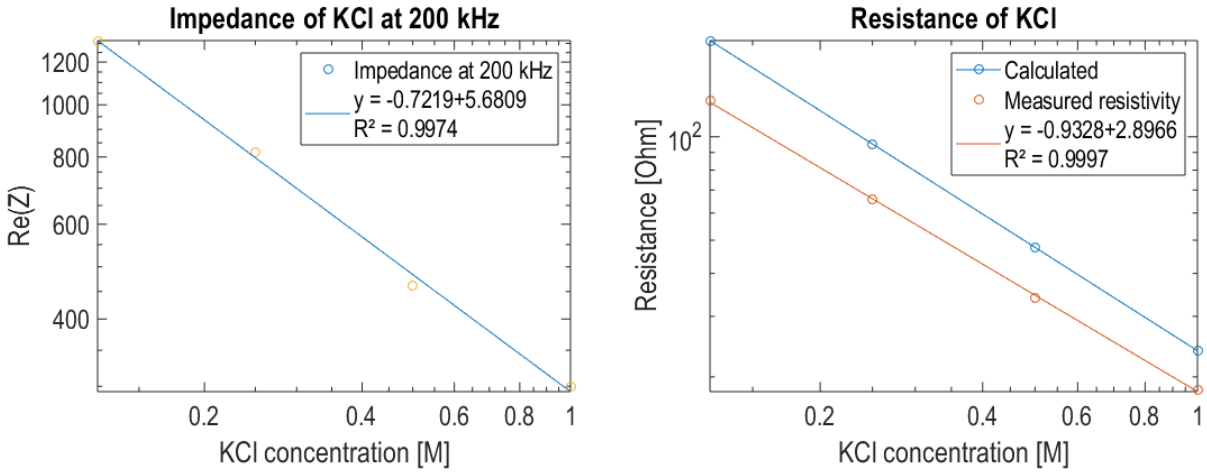

Figure 15: On the left the real impedance at 200 kHz against the KCl concentration plotted on a log-log scale to show the almost linear relation. On the right it can be compared to the resistance derived from the measured resistivity and calculated with the theoretical Molar conductivity of KCl.

Table 5: The resistance of the KCl solution between the working and the reference electrode derived via different methods. First, with the measured resistivity. Second, using the Molar conductivity of KCl. Third, the real impedance is taken at a frequency of 200 kHz.

KCl Concentration [mM]	Resisitivity [Ωm]	Resistance [Ω] 2.8 mm	Calculated Resistance [Ω] 2.8 mm	Impedance [Ω] at 200 kHz
1000	5.14	18.4	23.8	300
500	9.51	34.0	47.7	462
250	18.4	65.7	95.3	816
125	35.6	127	190.6	1315

5.3 Cyclic Voltammetry

Figure 16 shows the CV results in PBS while increasing the duration of pure nitrogen bubbling through the PBS. We expect there to be a decrease in the amount of current at the low end of the potentials since the reduction of oxygen takes place around -0.7 V[35]. By seeing the graph moving upwards, we can indeed say that the current decreases while nitrogen is bubbled longer through the solution, which points to less reduction of oxygen.

5.4 Amperometry

In Figure 17 the amperometry results are given of bubbling different nitrogen and air ratios through PBS. A more considerable current flow is expected at a higher concentration of air, which means a higher concentration of oxygen. Also, a change in slope is expected when the current is plotted against $\frac{1}{\sqrt{t}}$. The change in slope should be linear with the change in concentration following the Cottrell equation as explained in section 2.3. This is not the case when only waiting 10 minutes in between the measurements which can be seen in Appendix B where only the response changed after 3 measurements. The slopes of the graph at different concentrations are determined by doing a linear fit per concentration. The R^2 for these fits is between 0.9889 and 0.9984. Figure 17 shows a clear distinction between the measurements and a linear relation can be seen between the slope and the oxygen concentration in Figure 18.

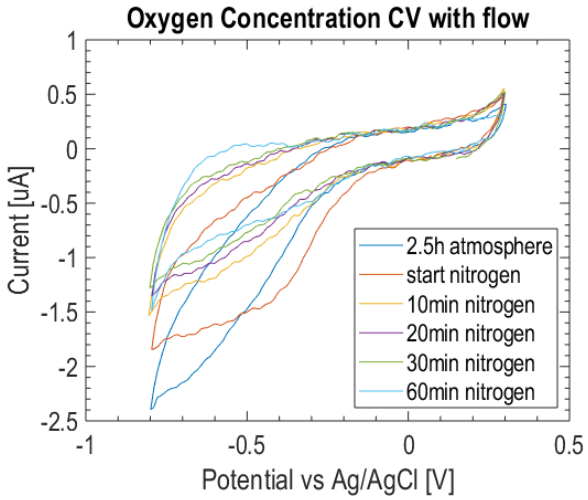

Figure 16: CV measured at different time intervals of a PBS solution with nitrogen gas flowing through it. The lowest peak of the graph moves upwards which points to less oxygen being reduced at those potentials.

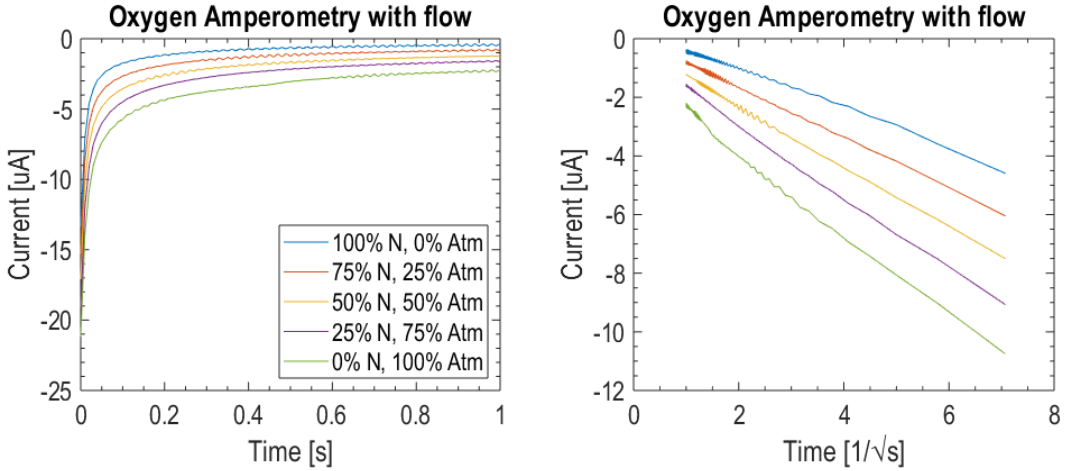

Figure 17: Amperometry results of varying oxygen concentrations flowing through PBS, the measurements were done after 30 minutes of bubbling the gas mixture. On the left side the raw measurements data and on the right side the current plotted against $\frac{1}{\sqrt{t}}$

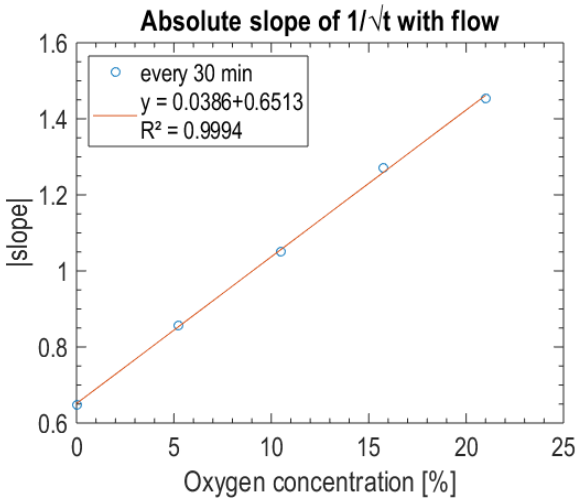

Figure 18: The slope of the current to $\frac{1}{\sqrt{t}}$ plotted against the oxygen concentration in the water measuring after 30 minutes of gas mixture flowing through the solution.

6 Discussion and Conclusion

The goal of this master project is to design a way of integrating electrochemical sensor read-out onto the Starterkit in a standardized and open manner, ensuring optimal signal quality and ease of use while maintaining a standalone character. During the design, the goals of the Starterkit and the ISO standard and the vision of electrical integration in the platform have been taken into account. This has led to a device of 35 x 38 mm that can fit on top of a 30 x 30 mm MFBB on the Starterkit. The electrodes are easily removable and there is only one micro-USB cable that is used for power and communication with the device. Proof of principle designs have been carried out to show if the device is capable of also doing electrochemical measurements on systems inside an MFBB.

The comparison to the BioLogic and simulations are very promising with only a minor deviation at the higher frequencies. Since this is the response that is expected with an extra inductance, the higher impedance at higher frequencies can be due to a parasitic inductance inside the circuit and/or the electrodes connected to the module. The BioLogic SP-300 has active cancellation of parasitics in its wires and circuit, and the simulation does not have it at all. This deviation can be expected from a device that is much smaller, costs less, and has fewer features. While the deviation is at higher frequencies where the double layer capacitance is not measured, it is not detrimental to have since it is a constant parasitic. This means that if you compare the measurements of the module against each other, there should be a constant offset, and you can still make comparative measurements. In the application for TEER measurement this means that a change in the cell layer over time can still be measured. To do quantitative measurements an extra step needs to be taken to make a calibration curve on which measurements can be evaluated. This is confirmed by the impedance measured of KCl. While the impedance is higher than the theoretical and measured resistance, in part due to the unknown electrochemical cell constant, the relation of the measurements is still linear on a log-log scale. Thus with a calibration curve, KCl concentrations can be derived from an unknown solution.

The results from the cyclic voltammetry show some noise, but this could be due to the peristaltic pump and, therefore, the pulsing flow along the electrodes. Still, the results show a change in the amount of oxygen reducing at the electrode. There were no perfect peaks measured for the oxygen reduction due to not sweeping down to lower potentials and the start of the reduction of other species in the solution. Therefore, the concentration cannot be derived from these results. In this instance, that is not necessary since, with chronoamperometry, the concentrations of oxygen can be determined. The CV results still show that this measurement technique is possible and could be used to determine the redox potentials of other species.

The chronoamperometry measurements clearly indicated the linear relation between the oxygen concentration and the slope of the $\frac{1}{\sqrt{t}}$ plot. Therefore, again, with calibration curves, unknown oxygen concentrations can be measured with the device.

Looking back at the goals mentioned in Table 2 can be evaluated. The module fits on the Starterkit using the existing connections of a 30 x 30 mm MFBB. During the proof-of-concept measurements, the device does not show significant noise inside the measured signals. Only a micro-USB cable is used to connect to the device. The electrodes can be easily connected and there is support for a wide range of electrodes. With the proof-of-concept experiments, it is shown that biological parameters could be measured, and this design is capable of adding electrochemical measurements to the Starterkit. The commercially available EmStat Pico has good support and documentation and can, therefore, be easily controlled via a computer program. By using off-the-shelf components and an open communication standard, the device can be easily replicated and improved. All together shows that the aim of the project was achieved by making a usable potentiostat that fits on the Starterkit.

7 Future prospects

Electrodes: During this project, the idea of using screen-printed electrodes with the EmStat Pico module has already been taken into account. Screen-printed electrodes are commonly used for testing wearable devices and could be very accessible in the Starterkit with this device. By using flexible PCB mass manufacturing, the shapes and positions of the electrodes can be cheaply made, whereafter the desired electrode materials can be deposited using electroplating or clean room sputtering techniques. A prototype of a screen-printed electrode with the module can be seen in Figure 19.

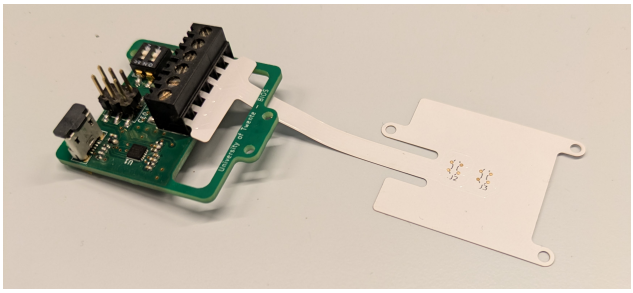

Figure 19: The Emstat Pico module together with a concept flexible PCB to be used as electrodes in an MFBB.

Integration: The footprint of the PCB right now exceeds the 30 x 30 mm standard for MFBBs which is not a problem on the Starterkit but could become a problem on other platforms. Therefore, the PCB could also be redesigned to fit those dimensions by using the EmStat Pico Core chip. This would provide more flexibility in the position of components and the space on the circuit board can be more optimally utilized.

Communication: Since this is the first version of the PCB for this device the functionality could also be increased by a redesign of the PCB. Since the vision of the Starterkit is to have more electronics integrated on the platform and still reduce the amount of wires needed, the communication of the module could be expanded. The I2C connections to the EmStat Pico Module could be exposed on external pins to increase compatibility with other peripherals. Bluetooth functionality could also be added so the data wires could be eliminated. This should be done in a stacked PCB approach, however, since a Bluetooth module takes up a lot of space.

Validation: To show more potential of the device the same electrode setup as shown in this report could be used to measure dopamine concentrations as described by Chen *et al.* [36]. Platinum could also be fictionalized with ionophores to measure the concentrations of specific ions by using the device's OCP measurements.

8 Acknowledgments

I want to thank my supervisors, Mathieu and Aniruddha, for their guidance and support throughout this project. Mathieu, thank you for extending my knowledge of electrochemistry, without which this project would not have come this far. Aniruddha, your daily supervision, insightful feedback, and assistance in the fabrication and assembly were crucial for this project.

I am grateful to everyone at the BIOS research chair for their kindness. Your willingness to answer my questions and offer support has made my experience during this project very enjoyable. Josh, especially, for your patience with my questions.

I thank my external supervisor, Dennis Alveringh, for his time and feedback on this project.

I want to thank Marten for his help soldering the components on the PCB. I greatly appreciate your skill and assistance.

Finally, I want to thank my parents and girlfriend for their support and encouragement. Listening to my drafts and concepts helped me organize my thoughts and stay motivated to write the report.

Thank you all for supporting me in completing my master's project!

References

[1] J. Orloff, F. Douglas, J. Pinheiro *et al.*, 'The future of drug development: Advancing clinical trial design', *Nature Reviews Drug Discovery*, vol. 8, no. 12, pp. 949–957, Dec. 2009, ISSN: 1474-1776, 1474-1784. DOI: 10.1038/nrd3025. [Online]. Available: https://www.nature.com/articles/nrd3025 (visited on 15/11/2024).

[2] 'Animals in science - european commission'. (19th Sep. 2024), [Online]. Available: https://environment.ec.europa.eu/topics/chemicals/animals-science_en (visited on 25/11/2024).

[3] R. Gallagher and T. Appenzeller, 'Beyond reductionism', *Science*, vol. 284, no. 5411, pp. 79–79, 2nd Apr. 1999, ISSN: 0036-8075, 1095-9203. DOI: 10.1126/science.284.5411.79. [Online]. Available: https://www.science.org/doi/10.1126/science.284.5411.79 (visited on 25/11/2024).

[4] A. D. Van Der Meer and A. Van Den Berg, 'Organs-on-chips: Breaking the in vitro impasse', *Integrative Biology*, vol. 4, no. 5, p. 461, 2012, ISSN: 1757-9694, 1757-9708. DOI: 10.1039/c2ib00176d. [Online]. Available: https://academic.oup.com/ib/article/4/5/461-470/5208384 (visited on 01/05/2024).

[5] D. Mark, S. Haeberle, G. Roth, F. Von Stetten and R. Zengerle, 'Microfluidic lab-on-a-chip platforms: Requirements, characteristics and applications', *Chemical Society Reviews*, vol. 39, no. 3, p. 1153, 2010, ISSN: 0306-0012, 1460-4744. DOI: 10.1039/b820557b. [Online]. Available: http://xlink.rsc.org/?DOI=b820557b (visited on 25/03/2024).

[6] C. M. Leung, P. De Haan, K. Ronaldson-Bouchard *et al.*, 'A guide to the organ-on-a-chip', *Nature Reviews Methods Primers*, vol. 2, no. 1, p. 33, 12th May 2022, ISSN: 2662-8449. DOI: 10.1038/s43586-022-00118-6. [Online]. Available: https://www.nature.com/articles/s43586-022-00118-6 (visited on 25/11/2024).

[7] 'ISO/IWA 23:2016(en), interoperability of microfluidic devices — guidelines for pitch spacing dimensions and initial device classification'. (2016), [Online]. Available: https://dgn.isolutions.iso.org/obp/ui#iso:std:iso:iwa:23:ed-1:v1:en (visited on 24/05/2024).

[8] A. Manz, N. Graber and H. Widmer, 'Miniaturized total chemical analysis systems: A novel concept for chemical sensing', *Sensors and Actuators B: Chemical*, vol. 1, no. 1, pp. 244–248, Jan. 1990, ISSN: 09254005. DOI: 10.1016/0925-4005(90)80209-I. [Online]. Available: https://linkinghub.elsevier.com/retrieve/pii/092540059080209I (visited on 22/05/2024).

[9] T. Lammerink, V. Spiering, M. Elwenspoek, J. Fluitman and A. Van Den Berg, 'Modular concept for fluid handling systems. a demonstrator micro analysis system', in *Proceedings of Ninth International Workshop on Micro Electromechanical Systems*, San Diego, CA, USA: IEEE, 1996, pp. 389–394, ISBN: 978-0-7803-2985-0. DOI: 10.1109/MEMSYS.1996.494013. [Online]. Available: http://ieeexplore.ieee.org/document/494013/ (visited on 25/03/2024).

[10] C. G. J. Schabmueller, M. Koch, A. G. R. Evans and A. Brunnschweiler, 'Design and fabrication of a microfluidic circuitboard', *Journal of Micromechanics and Microengineering*, vol. 9, no. 2, pp. 176–179, 1st Jun. 1999, ISSN: 0960-1317, 1361-6439. DOI: 10.1088/0960-1317/9/2/318. [Online]. Available: https://iopscience.iop.org/article/10.1088/0960-1317/9/2/318 (visited on 25/03/2024).

[11] M. J. Gilde, H. Van Den Vlekkert, H. Leeuwis and A. Prak, 'Modular design approach for MicroFluidic systems', *TechConnect Briefs*, vol. 1, Technical Proceedings of the 2005 NSTI Nanotechnology Conference and Trade Show, Volume 1, pp. 684–687, 8th May 2005. [Online]. Available: https://briefs.techconnect.org/papers/modular-design-approaches-for-microfluidic-systems/.

[12] S. Dekker, 'Industry-supported, and standardized modular platform : Interconnecting fluidic circuit board and microfluidic building blocks', ISBN: 9789036546119, Ph.D. dissertation, University of Twente, Enschede, The Netherlands, 9th Nov. 2018. DOI: 10.3990/1.9789036546119. [Online]. Available: http://purl.org/utwente/doi/10.3990/1.9789036546119 (visited on 08/04/2024).

[13] S. Dekker, P. K. Isgor, T. Feijten, L. I. Segerink and M. Odijk, 'From chip-in-a-lab to lab-on-a-chip: A portable coulter counter using a modular platform', *Microsystems & Nanoengineering*, vol. 4, no. 1, p. 34, 19th Nov. 2018, ISSN: 2055-7434. DOI: 10.1038/s41378-018-0034-1. [Online]. Available: https://www.nature.com/articles/s41378-018-0034-1 (visited on 19/03/2024).

[14] E. Safai, *Translational organ-on-chip platform (TOP) design rules (TDRs)*, in collab. with University Of Twente, Faculty Of Science And Technology (TNW), Applied Stem Cell Technologies (AST), version 2, 17th May 2024. DOI: 10.4121/2558BD4C-D7AD-4E17-BC54-8C335B4C1C01.V2. [Online]. Available: https://data.4tu.nl/datasets/2558bd4c-d7ad-4e17-bc54-8c335b4c1c01/2 (visited on 27/05/2024).

[15] ISO/TC 48, *Microfluidic devices - interoperability requirements for dimensions, connections and initial device classification*, version ISO 22916:2022(E), Jan. 2022. [Online]. Available: https://www.iso.org/cms/%20render/live/en/sites/isoorg/contents/data/standard/07/41/74157.html?browse=tc.

[16] S. Fuchs, S. Johansson, A. Ø. Tjell, G. Werr, T. Mayr and M. Tenje, 'In-line analysis of organ-on-chip systems with sensors: Integration, fabrication, challenges, and potential', *ACS Biomaterials Science & Engineering*, vol. 7, no. 7, pp. 2926–2948, 12th Jul. 2021, ISSN: 2373-9878, 2373-9878. DOI: 10.1021/acsbiomaterials.0c01110. [Online]. Available: https://pubs.acs.org/doi/10.1021/acsbiomaterials.0c01110 (visited on 22/03/2024).

[17] C.-S. Lee, S. Kim and M. Kim, 'Ion-sensitive field-effect transistor for biological sensing', *Sensors*, vol. 9, no. 9, pp. 7111–7131, 7th Sep. 2009, ISSN: 1424-8220. DOI: 10.3390/s90907111. [Online]. Available: http://www.mdpi.com/1424-8220/9/9/7111 (visited on 05/04/2024).

[18] S. Sinha and T. Pal, 'A comprehensive review of FET-based pH sensors: Materials, fabrication technologies, and modeling', *Electrochemical Science Advances*, vol. 2, no. 5, e2100147, Oct. 2022, ISSN: 2698-5977, 2698-5977. DOI: 10.1002/elsa.202100147. [Online]. Available: https://chemistry-europe.onlinelibrary.wiley.com/doi/10.1002/elsa.202100147 (visited on 04/06/2024).

[19] S. Głab, A. Hulanicki, G. Edwall and F. Ingman, 'Metal-metal oxide and metal oxide electrodes as pH sensors', *Critical Reviews in Analytical Chemistry*, vol. 21, no. 1, pp. 29–47, Aug. 1989, ISSN: 1040-8347, 1547-6510. DOI: 10.1080/10408348908048815. [Online]. Available: https://www.tandfonline.com/doi/full/10.1080/10408348908048815 (visited on 04/06/2024).

[20] L. Manjakkal, D. Szwagierczak and R. Dahiya, 'Metal oxides based electrochemical pH sensors: Current progress and future perspectives', *Progress in Materials Science*, vol. 109, p. 100 635, Apr. 2020, ISSN: 00796425. DOI: 10.1016/j.pmatsci.2019.100635. [Online]. Available: https://linkinghub.elsevier.com/retrieve/pii/S0079642519301173 (visited on 05/04/2024).

[21] M. Azimzadeh, P. Khashayar, M. Amereh, N. Tasnim, M. Hoorfar and M. Akbari, 'Microfluidic-based oxygen (o2) sensors for on-chip monitoring of cell, tissue and organ metabolism', *Biosensors*, vol. 12, no. 1, p. 6, 22nd Dec. 2021, ISSN: 2079-6374. DOI: 10.3390/bios12010006. [Online]. Available: https://www.mdpi.com/2079-6374/12/1/6 (visited on 23/05/2024).

[22] K. R. Choi, X. V. Chen, J. Hu and P. Bühlmann, 'Solid-contact pH sensor with covalent attachment of ionophores and ionic sites to a poly(decyl methacrylate) matrix', *Analytical Chemistry*, vol. 93, no. 50, pp. 16 899–16 905, 21st Dec. 2021, ISSN: 0003-2700, 1520-6882. DOI: 10.1021/acs.analchem.1c03985. [Online]. Available: https://pubs.acs.org/doi/10.1021/acs.analchem.1c03985 (visited on 15/07/2024).

[23] J. Zhai, D. Yuan and X. Xie, 'Ionophore-based ion-selective electrodes: Signal transduction and amplification from potentiometry', *Sensors & Diagnostics*, vol. 1, no. 2, pp. 213–221, 2022, ISSN: 2635-0998. DOI: 10.1039/D1SD00055A. [Online]. Available: https://xlink.rsc.org/?DOI=D1SD00055A (visited on 29/08/2024).

[24] M. A. Holzreuter and L. I. Segerink, 'Innovative electrode and chip designs for transendothelial electrical resistance measurements in organs-on-chips', *Lab on a Chip*, vol. 24, no. 5, pp. 1121–1134, 2024, ISSN: 1473-0197, 1473-0189. DOI: 10.1039/D3LC00901G. [Online]. Available: http://xlink.rsc.org/?DOI=D3LC00901G (visited on 21/03/2024).

[25] M. W. Van Der Helm, O. Y. F. Henry, A. Bein *et al.*, 'Non-invasive sensing of transepithelial barrier function and tissue differentiation in organs-on-chips using impedance spectroscopy', *Lab on a Chip*, vol. 19, no. 3, pp. 452–463, 2019, ISSN: 1473-0197, 1473-0189. DOI: 10.1039/C8LC00129D. [Online]. Available: http://xlink.rsc.org/?DOI=C8LC00129D (visited on 19/03/2024).

[26] E. Bossink, 'Recreating the gut on-chip : Sensors and fabrication technologies for aerobic intestinal host - anaerobic microbiota research', ISBN: 9789036553995, Ph.D. dissertation, University of Twente, Enschede, The Netherlands, 8th Jul. 2022. DOI: 10.3990/1.9789036553995. [Online]. Available: http://purl.org/utwente/doi/10.3990/1.9789036553995 (visited on 05/06/2024).

[27] R. A. Dorledo De Faria, L. G. Dias Heneine, T. Matencio and Y. Messaddeq, 'Faradaic and non-faradaic electrochemical impedance spectroscopy as transduction techniques for sensing applications', *International Journal of Biosensors & Bioelectronics*, vol. 5, no. 1, 28th Feb. 2019, ISSN: 25732838. DOI: 10.15406/ijbsbe.2019.05.00148. [Online]. Available: https://medcraveonline.com/IJBSBE/faradaic-and-non-faradaic-electrochemical-impedance-spectroscopy-as-transduction-techniques-for-sensing-applications.html (visited on 26/11/2024).

[28] A. C. Lazanas and M. I. Prodromidis, 'Electrochemical impedance spectroscopy—a tutorial', *ACS Measurement Science Au*, vol. 3, no. 3, pp. 162–193, 21st Jun. 2023, ISSN: 2694-250X, 2694-250X. DOI: 10.1021/acsmeasuresciau.2c00070. [Online]. Available: https://pubs.acs.org/doi/10.1021/acsmeasuresciau.2c00070 (visited on 26/11/2024).

[29] P. M. Biesheuvel, S. Porada and J. E. Dykstra, *The difference between faradaic and non-faradaic electrode processes*, 11th Jan. 2021. DOI: 10.48550/arXiv.1809.02930. arXiv: 1809.02930[physics]. [Online]. Available: http://arxiv.org/abs/1809.02930 (visited on 26/11/2024).

[30] N. Elgrishi, K. J. Rountree, B. D. McCarthy, E. S. Rountree, T. T. Eisenhart and J. L. Dempsey, 'A practical beginner's guide to cyclic voltammetry', *Journal of Chemical Education*, vol. 95, no. 2, pp. 197–206, 13th Feb. 2018, ISSN: 0021-9584, 1938-1328. DOI: 10.1021/acs.jchemed.7b00361. [Online]. Available: https://pubs.acs.org/doi/10.1021/acs.jchemed.7b00361 (visited on 03/09/2024).

[31] M. N. Islam and R. B. Channon, 'Electrochemical sensors', in *Bioengineering Innovative Solutions for Cancer*, Elsevier, 2018, pp. 47–71, ISBN: 978-0-12-813886-1. DOI: 10.1016/B978-0-12-813886-1.00004-8. [Online]. Available: https://linkinghub.elsevier.com/retrieve/pii/B9780128138861000048 (visited on 26/11/2024).

[32] P. Bhatnagar and F. Beyette, 'Microcontroller-based electrochemical impedance spectroscopy for wearable health monitoring systems', in *2015 IEEE 58th International Midwest Symposium on Circuits and Systems (MWSCAS)*, Fort Collins, CO, USA: IEEE, Aug. 2015, pp. 1–4, ISBN: 978-1-4673-6558-1. DOI: 10.1109/MWSCAS.2015.7282197. [Online]. Available: http://ieeexplore.ieee.org/document/7282197/ (visited on 24/04/2024).

[33] 'EmStat pico module', PalmSens. (), [Online]. Available: https://www.palmsens.com/product/oem-emstat-pico-module/ (visited on 20/06/2024).

[34] M. W. Shinwari, D. Zhitomirsky, I. A. Deen, P. R. Selvaganapathy, M. J. Deen and D. Landheer, 'Microfabricated reference electrodes and their biosensing applications', *Sensors*, vol. 10, no. 3, pp. 1679–1715, 2nd Mar. 2010, ISSN: 1424-8220. DOI: 10.3390/s100301679. [Online]. Available: https://www.mdpi.com/1424-8220/10/3/1679 (visited on 27/11/2024).

[35] E. I. Rogers, A. M. O'Mahony, L. Aldous and R. G. Compton, '(invited) amperometric gas detection using room temperature ionic liquid solvents', *ECS Transactions*, vol. 33, no. 7, pp. 473–502, 1st Oct. 2010, ISSN: 1938-5862, 1938-6737. DOI: 10.1149/1.3484806. [Online]. Available: https://iopscience.iop.org/article/10.1149/1.3484806 (visited on 27/11/2024).

[36] X. Chen, J. Chen, H. Dong, Q. Yu, S. Zhang and H. Chen, 'Sensitive detection of dopamine using a platinum microelectrode modified by reduced graphene oxide and gold nanoparticles', *Journal of Electroanalytical Chemistry*, vol. 848, p. 113 244, Sep. 2019, ISSN: 15726657. DOI: 10.1016/j.jelechem.2019.113244. [Online]. Available: https://linkinghub.elsevier.com/retrieve/pii/S1572665719305120 (visited on 14/10/2024).

During the preparation of this work, the author used ChatGPT to brainstorm ideas and generate possible writing structures, Perplexity to search for sources to answer more specific questions, and Grammarly to improve the writing of this report. After using these tools/services, the author reviewed and edited the content as needed and takes full responsibility for the content of the work.

A Stability of quasi-reference Ag/AgCl

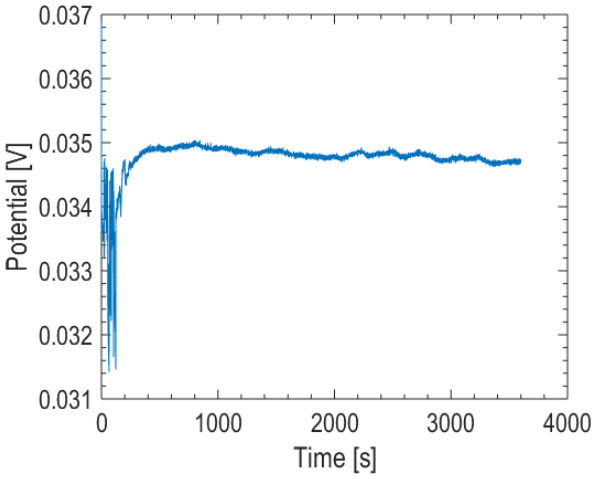

Figure 20: The potential of the quasi-reference Ag/AgCl electrode measured for 1 hour against a KCl saturated Ag/AgCl electrode. The maximum change in potential in one hour is 1.2 mV, not considering the settling of the measurement and electrode in the first two minutes.

B Amperometry Results

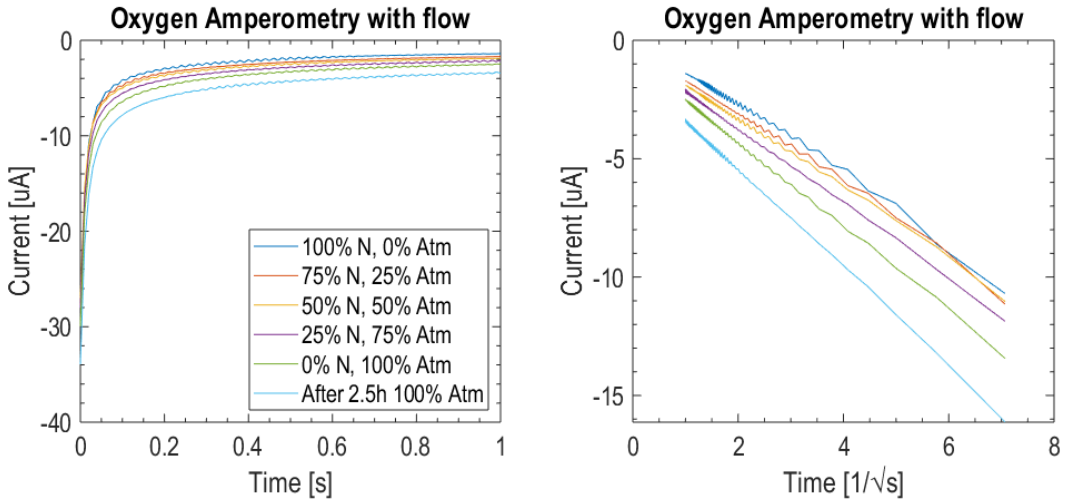

Figure 21: Amperometry results of varying oxygen concentrations flowing through PBS. The measurements were done after 10 minutes of bubbling the gas mixture. On the left side, the raw measurements data, and on the right side, the current plotted against $\frac{1}{\sqrt{t}}$.

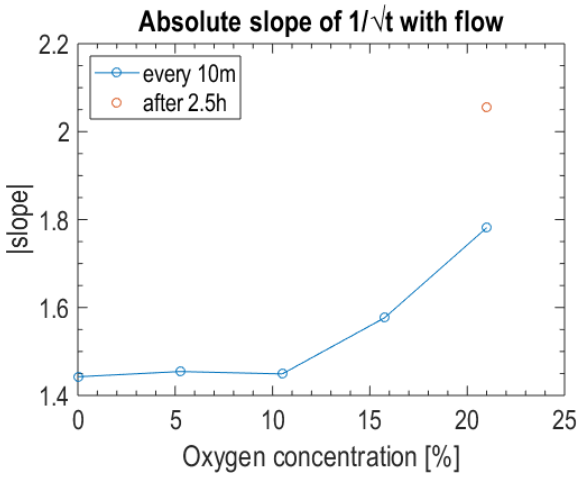

Figure 22: The slope of the current to $\frac{1}{\sqrt{t}}$ plotted against the oxygen concentration in the water measuring after 10 minutes of the gas mixture flowing through the solution.

C Circuit Design

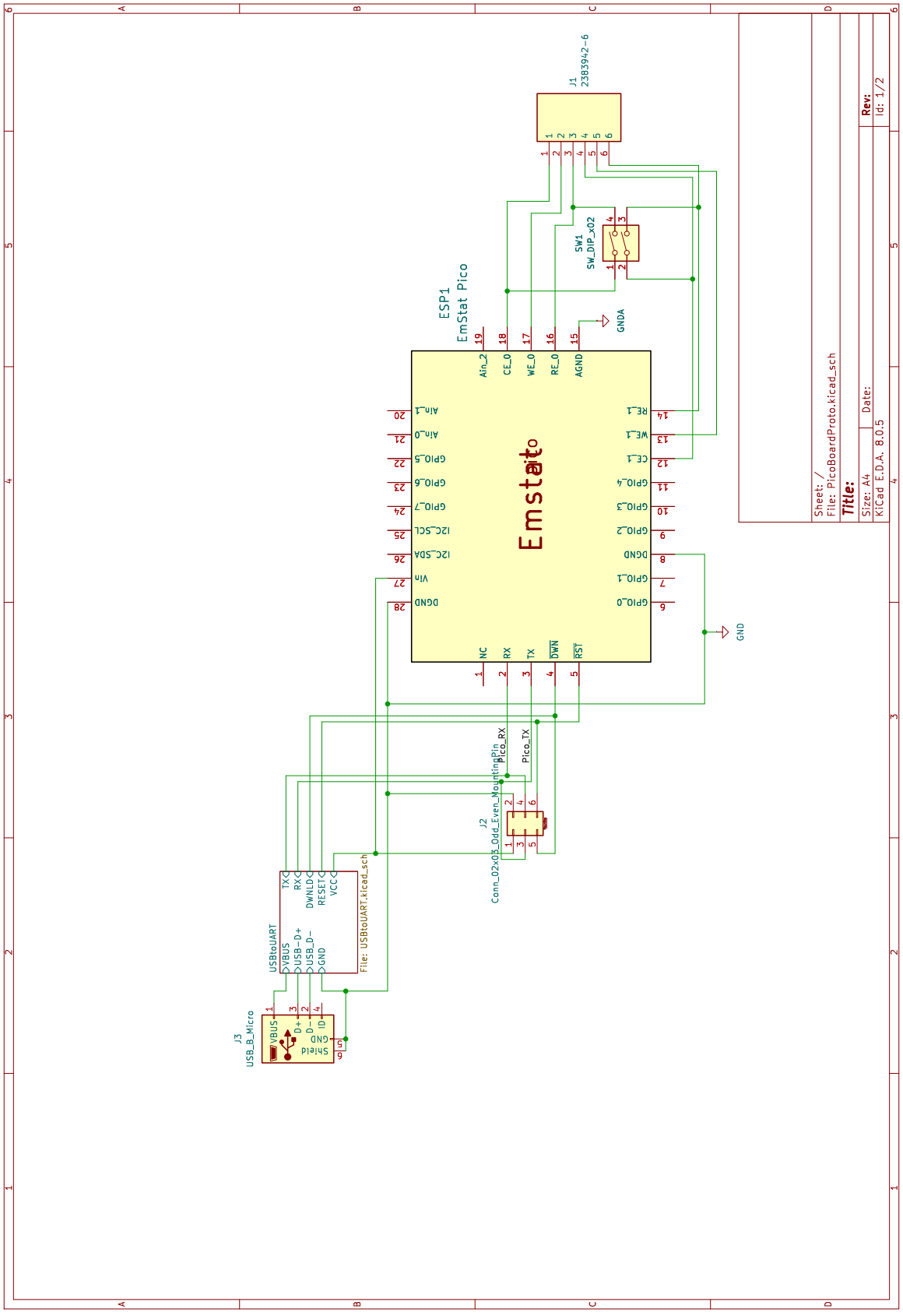

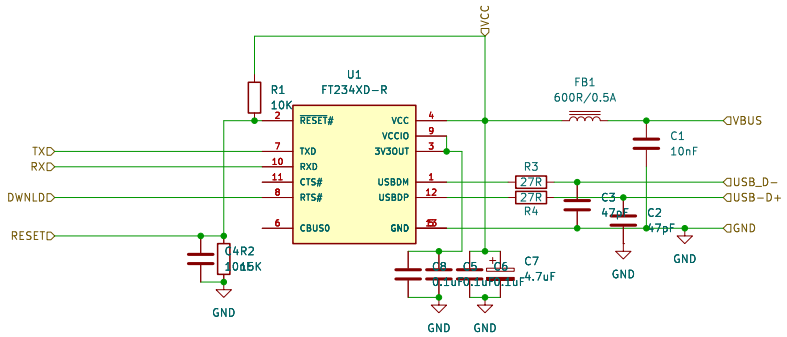

Sheet: /USBtoUART/		
File: USBtoUART.kicad_sch		
Title:		
Size: A4	Date:	**Rev:**
KiCad E.D.A. 8.0.5		Id: 2/2